In Vivo Brain Region-specific TSPO Imaging by PET/MRI [18F]FEPPA

Chi-Wei Chang
Taipei Veterans General Hospital
Chuang-Hsin Chiu
Tri-Service General Hospital
Ming-Hsien Lin
Cheng Hsin Hospital
Hung-Ming Wu
Changhua Christian Hospital
Tsung-Hsun Yu
National Yang-Ming University
Pao-Yeh Wang
National Yang-Ming University
Yu-Yeh Kuo
National Yang-Ming University
Ya-Yao Huang
National Taiwan University Hospital
Chyng-Yann Shiue
National Taiwan University Hospital
Wen-Sheng Huang
Taipei Veterans General Hospital
Skye Hsin-Hsien Yeh (skyeyeh@live.com)
National Yang-Ming University https://orcid.org/0000-0002-7495-1146

Original research

Keywords: [18F]FEPPA, neuroinflammation, TSPO, animal PET/MR imaging

Posted Date: December 1st, 2020

DOI: https://doi.org/10.21203/rs.3.rs-116184/v1

Version of Record: A version of this preprint was published at EJNMMI Research on March 16th, 2021.
See the published version at https://doi.org/10.1186/s13550-021-00768-9.

in vivo brain region-specific TSPO imaging by PET/MRI [^{18}F]FEPPA

Chi-Wei Chang[1,2,3], Chuang-Hsin Chiu[4a], Ming Hsien Lin[5], Hung-Ming Wu[6], Tsung-Hsun Yu[7], Pao-Yeh Wang[7], Yu-Yeh Kuo[1], Ya-Yao Huang[8,9], Chyng-Yann Shiue[9,10], Wen-Sheng Huang[1,2b], Skye Hsin-Hsien Yeh[7*]

[1]Department of Nuclear Medicine, Taipei Veterans General Hospital, Taipei, Taiwan

[2]Department of Medical Imaging and Radiological Technology, The Institute of Radiological Sciences, Tzu Chi University of Science and Technology

[3]Department of Biomedical Engineering and Environmental Sciences, National Tsinghua University, Hsinchu,Taiwan

[4]Department of Nuclear Medicine, Tri-Service General Hospital, Taipei, Taiwan

[5]Department of Nuclear Medicine, Cheng Hsin General Hospital, Taipei, Taiwan

[6]Department of Neurology, Changhua Christian Hospital, No.135, Nanhsiao Street, Changhua, 500m Taiwan;

[7]Brain Research Center, National Yang-Ming University, Taipei, Taiwan.

[8]PET Center, Department of Nuclear Medicine, National Taiwan University Hospital, 7, Chung-Shan S. Road, Taipei, 100, Taiwan

[9] Molecular Imaging Center, National Taiwan University, No. 1, Sec. 4, Roosevelt Road, Taipei, 106, Taiwan

[10] PET Center, Department of Nuclear Medicine, Tri-Service General Hospital 325 Sec. 2, Cheng-Kung Road, Neihu 114, Taipei, Taiwan

[a]Equal contribution as first author

[b]co-corresponding author

Running Title: PET [^{18}F]FEPPA imaging in central and peripheral tissue

*Corresponding author:

Skye Hsin-Hsien Yeh, Ph.D.

Tel: 886-2-2821-3496; Fax: 886-2-2822-3970

E-mail: skyeyeh@live.com

Mailing address:

Brain Research Center, National Yang-Ming University, Taipei, Taiwan.

No.155, Sec.2, Linong Street, Taipei, 112 Taiwan

Abstract

Background: Expression of translocator protein (TSPO) on the outer mitochondrial membrane of activated microglia is strongly associated with neuroinflammation. The second-generation PET ligand [^{18}F]FEPPA specifically binds TSPO to enable *in vivo* visualization and quantification of neuroinflammation. We optimized an fully automated radiosynthesis method and evaluated the utility of [^{18}F]FEPPA, the second-generation PET ligand specifically binds TSPO, in a mouse model of systemic LPS challenge to detect TSPO-associated signals of central and peripheral inflammation. *In vivo* dynamic PET/MR imaging was performed in LPS-induced and control mice after [^{18}F]FEPPA administration. The relationship between the [^{18}F]FEPPA signal and the dose of LPS was assessed. The cytokine levels (i.e. TNF-α, Il-1β, Il-6) in LPS-induced mice were measured by RT-PCR. Standard uptake value (SUV), total volume of distribution (VT) and area under the curve (AUC) were determined based on the metabolite-uncorrected plasma input function. Western blotting and immunostaining were used to measure TSPO expression in the brain.

Results: The fully automated [^{18}F]FEPPA radiosynthesis produced an uncorrected radiochemical yield of 30 ± 2% within 80 min, with a radiochemical purity greater than 99% and specific activity of 148.9–216.8 GBq/μmol. Significant differences were observed in the brain after [^{18}F]FEPPA administration: SUV, VT, and AUC were 1.61

± 0.1, 1.25 ± 0.12, and 1.58 ± 0.09-fold higher in LPS-injected mice than controls. TNF-α, Il-1β and Il-6 mRNA levels were also elevated in the brains of LPS-injected mice. Western blotting revealed TSPO ($p<0.05$) and Iba-1 ($p<0.01$) were upregulated in the brain after LPS administration. In LPS-injected mice, TSPO immunoactivity colocalized with Iba-1 in the cerebrum and TSPO was significantly overexpressed in the hippocampus and cerebellum. The peripheral organs (heart, lung) of LPS-injected mice had higher [^{18}F]FEPPA signal-to-noise ratios than control mice.

Conclusions: Based on the robust data on ligand specificity and selectivity in both central and peripheral tissues using 7T PET/MR imaging, we demonstrate that the high affinity, stability and high-contrast visualization indicate detection of TSPO using [^{18}F]FEPPA represents a promising, specific biomarker for early diagnosis and neuropathological follow-up of neuroinflammatory processes.

Keywords: [^{18}F]FEPPA, neuroinflammation, TSPO, animal PET/MR imaging

Introduction

The 18-kDa mitochondrial translocator protein (TSPO), originally named peripheral-type benzodiazepine receptor (PBR), plays important roles in several physiological processes, including steroidogenesis (1) (2), inflammation (3) and cell proliferation (4). TSPO is endogenously expressed at high levels in some peripheral tissues, including the adrenal gland, heart, lung, kidney and testis (3). However, TSPO is expressed at very low levels in the central nervous system (CNS) under normal conditions, and limited to glial cells (astrocytes and microglia) (3) (5) (6).

Neuroinflammation is characterized by the activation of neuroimmune cells and implicated in the pathogenesis of several neurodegenerative diseases. Glial cells are activated in response to brain injury or neuroinflammation, and activated microglial/macrophages are associated with dramatically increased expression of TSPO (7). High expression of TSPO in activated microglia has been reported in several neurodegenerative diseases, including Alzheimer's disease (8), Huntington's disease (9), ischemic stroke (10), multiple sclerosis (11) and epilepsy (12), which indicates TSPO plays essential roles in the progression of these diseases. Therefore, TSPO is considered to represent a relevant molecular marker for neuroinflammation and could possibly be an attractive therapeutic target. Thus, a specific biomarker for TSPO may

improve early diagnosis and neuropathological follow-up after therapy, and even enable pharmacological screening of TSPO ligands.

Given the enhanced expression of TSPO in inflammatory cells in the injured brain, neuroimaging such as positron emission tomography (PET) or single-photon emission computed tomography (SPECT) employing TSPO radioligands may provide valuable approaches to track and quantify brain inflammation, and thereby assess the effectiveness of therapeutic interventions in real-time. [^{11}C]PK11195 was the first identified and is the most studied TSPO radioligand; however, due to its high lipophilicity, radiolabeled PK11195 exhibits high non-specific binding and leads to a poor signal-to-noise ratio, which complicates quantification(13). Numerous second-generation TSPO-PET tracers have been developed to address these limitations, including [^{11}C]CLINME(14), [^{11}C]DAA1106(15), [^{11}C]SSR180575(16),(17), [^{18}F]FMDAA1106 (18, 19), [^{18}F]PBR01(20), [^{18}F]PBR06(21), [^{18}F]PBR111(22), [^{11}C/^{18}F]PBR28 (23), [^{11}C]DPA-713 (24), [^{18}F]DPA-714 (25), [^{18}F]FEAC/FEDAC (26), [^{18}F]FEPPA (27) (28) (29, 30) and [^{18}F]GE-180 (31).

Radiolabeled-TSPO ligands have been widely used to study the role of TSPO in animal models of chemical-induced neurotoxicity—such as lipopolysaccharide (LPS)-induced neurotoxicity—and also in models of human neurodegenerative disorders. These

promising preclinical studies prompted clinical studies of TSPO ligands to detect neuroinflammation; however, these clinical studies produced mixed results. The first-generation radioligand [^{11}C]PK-11195 was reported to lead to higher TSPO PET signals in the brains of patients with amyotrophic lateral sclerosis (32), Alzheimer's disease (8), Parkinson's disease (10), or individuals at risk of Huntington's disease (33) compared to healthy controls. However, other TSPO PET studies using [^{11}C]DAA1106 in cognitive impairment-dementia, [^{18}F]FEDAA1106 in multiple sclerosis (19), and [^{18}F]DPA-714 (34) or [^{18}F]FEDAA1106 (35) in Alzheimer's disease reported no significant differences. The second-generation TSPO ligand [^{18}F]-N-(2-(2-fluoroethoxy)benzyl)-N-(4-phenoxypyridin-3-yl) acetamide ([^{18}F]FEPPA) has superior properties to other ligands, including an 18-fold higher affinity than [^{11}C]PK-11195 and metabolic stability *in vivo* (27) (36).

Administration of LPS—mainly by local intracerebral injection—is widely used to induce neuroinflammation in animals models for TSPO PET or neuroinflammation studies (37) (38) (39). The metabolism and total volume distribution (VT) of [^{18}F]FEPPA in the brain were previously determined in a murine model of systemic LPS-induced neuroinflammation (30).

However, even though the LPS-induced model is widely used, detection of regional-specific binding of TPSO in the brain using PET and the dynamic distribution

of TSPO in the peripheral organs remain unclear in rodent LPS models. Furthermore, the effectiveness of [^{18}F]FEPPA as a PET ligand in animals injected with varied doses of LPS requires further investigation. Moreover, an automated [^{18}F]FEPPA radiosynthesis protocol that meets Good Manufacturing Practice is required for clinical purposes.

The overall aims of this study were to (i) optimize a fully automated radiosynthesis protocol for [^{18}F]FEPPA on the Eckert-Ziegler modular system (Eckert-Ziegler, Berlin, Germany); (ii) assess the regional-specific distribution of [^{18}F]FEPPA in various brain regions and peripheral organs in mice with LPS-induced neuroinflammation; and (iii) quantify the dose-dependence of the relationship between the dose of LPS and [^{18}F]FEPPA PET signals *in vivo*.

Materials and Methods

Optimized radiochemical synthesis of [^{18}F]FEPPA

Reagents

All reagents and solvents were purchased from Huayi Isotopes Inc. (Suzhou, China) or Sigma-Aldrich (St. Louis, MO, USA) and used without further purification. Sep-Pak®Light QMA cartridges and tC18 plus Sep-Pak cartridges were obtained from

Waters Corporation (Milford, MA, USA). The tosylated precursor of [18F]FEPPA, (2-(2-((N-4-phenoxypyridin-3-yl)acetamido)methyl)phenoxy)ethyl 4-methylbenzenesulfonate), and authentic FEPPA, N-(2-(2-fluoroethoxy)benzyl)-N-(4-phenoxypyridin-3-yl)acetamide, were purchased from Huayi Isotopes Inc. [^{18}F]fluoride ions were produced via the [18O(p,n)18F] nuclear reaction using a Scanditronix MC 17 cyclotron (Uppsala, Sweden). The radioactivity of the final product was measured with a dose calibrator (Capintec CRC-15R, Capintec, NJ, USA).

Radiosynthesis was performed using an Eckert-Ziegler modular system (Eckert-Ziegler, Berlin, Germany) and radiochemical yields were determined with a dose calibrator. Radioactive mixtures were purified by semi-preparative high-performance liquid chromatography (HPLC) using a Knauer pump P 2.1S (Knauer Corp., Berlin, Germany), Knauer UV/VIS detector UVD 2.1S (Knauer Corp.) and pin-diode radiodetector (Eckert-Ziegler). Quality control for the final product was performed by analytical HPLC using a Waters 2695 pump, Waters 2489 UV/VIS (254 nm) detector (Waters Corporation) and FC-4000 dual BGO coincidence detector (Bioscan, Inc., Washington, DC, USA). The amount of organic solvent was determined by gas chromatography (Varian Inc., Palo Alto, CA, USA).

Radiosynthesis

Radiosynthesis of [^{18}F]FEPPA was performed using an Eckert-Ziegler modular system and a tosylated precursor via a one-step fluorine nucleophilic aliphatic substitution, based on a previously described radiosynthesis (27) (**Figure 1**). The reagents used in the automated in-house reaction sequence are listed in **Suppl.Table 1**.

The aqueous [^{18}F]fluoride target solution was loaded onto a pre-conditioned QMA Sep-Pak® Light QMA cartridge (Waters Corporation). Concentrated [18F]fluoride was eluted into the reactor using 1.1 mL of a mixture of K_2CO_3 (2.75 mg) and Kryptofix (K222, 10.56 mg; CH3CN:H2O, 4:1, *v/v*). The solvents were evaporated under reduced pressure at 120 °C for 10 min. Five micrograms of the tosylated precursor (2-(2-((N-4-phenoxypyridin-3-yl)acetamido)methyl)phenoxy)ethyl 4-methylbenzenesulfonate) in acetonitrile (0.6 mL) was added to the dry residue containing the K222/potassium [^{18}F]fluoride complex, and the mixture was heated to 90 °C for 10 min and cooled. The radiolabeling reaction was stopped by adding 2 mL of the mobile phase CH_3CN:water (1:1 *v/v*) + 0.5% phosphoric acid into the reactor, and the solution was transferred into the injection loop. Purification was carried out by semi-preparative HPLC (column YMC-Actus Triart C18 250×20 mm I.D S-5 µm, 12 nm; Kyoto, Japan) in an isocratic (1:1 *v/v*) solution of CH3CN:water containing 0.5% phosphoric acid at a flow rate of 6 mL/min. The fraction containing [^{18}F]FEPPA was collected at 13-14 min and mixed with 40 mL of water. [^{18}F]FEPPA was subsequently trapped on a pre-conditioned (10

mL ethanol and 20 mL water) tC18plus SepPak cartridge, and the acetonitrile was washed off by rinsing the tC18plus SepPak cartridge with water. The product ([18F]FEPPA) was eluted with ethanol (0.9 mL) and formulated in normal saline (10 mL). The radiotracer solution was finally passed through a 0.22 μm Millipore filter into a sterile vial for *in vivo* experiments. The product was diluted in saline to obtain a volume activity of 2.2–2.8 GBq/mL.

Quality control

Radiochemical and chemical purity, stability and molar activity were assessed by analytical HPLC. The molar activity of the radiotracer was quantified by measuring the radioactivity injected and deriving the concentration of FEPPA in the sample by UV detection.

The identity of the labeled compound [^{18}F]FEPPA was confirmed by co-injection with a non-radioactive FEPPA standard. The concentration of FEPPA in the radioactive sample was obtained from the UV-peak area ratio for the radioactive product and the standard solution. Analytical HPLC was performed on a Nova-pak C18 column (300 × 3.9 mm, 4 □m) in 50 mM $(NH_4)H_2PO_4$:CH_3CN (1:1) at 1 mL/min using a Waters Corporation 2695 pump with a multi-wavelength 2489 UV Detector (Waters Corporation) in series with a Bioscan FC-4000 dual BGO coincidence detector

(Bioscan, Inc., Washington, DC, USA). A delay time of 12 s was observed between the two detectors.

Animals

Eight to nine-week-old male C57BL/6 mice were housed with free access to water and maintained under controlled temperature (22 ± 2˚C) and humidity (55-65%) under a 12-h light/dark cycle. All animal experiments were approved in advance by the National Yang-Ming University Institutional Animal Care and Use Committee (IACUC No: 1050910) and animal study was performed according to the Guidelines for Animal Experimentation of National Yang-Ming University.

LPS-induced mouse model

The mice in the LPS group were intraperitoneally injected with a single dose of 0.625, 1.25, 2.5 or 5 mg/kg LPS (*Escherichia coli*, strain O111:B4; Calbiochem, San Diego, CA, USA) to induce systemic inflammation. The control group were intraperitoneally injected with 0.9% NaCl. *In vivo* or *in vitro* assessments were performed 3 h or 24 h after administration of LPS.

***In vivo* PET/MRI imaging and imaging analysis**

Before PET/MR imaging acquisition, the mice were anesthetized by passive inhalation of a mixture of isoflurane and oxygen (5% isoflurane for induction and 2% for maintenance). A fiber-optic temperature probe was inserted into the rectum to monitor the core temperature of the mice, then each animal was gently positioned in the MR cradle and the MRI coil was secured around the head. A warm water blanket was positioned to maintain the core temperature of the animals, then the mice were positioned inside the scanner. The depth of anesthesia, pulse and respiration were monitored constantly during the imaging procedure; in the unlikely event that an animal regained consciousness, the scanning was immediately stopped and the animal was removed from the scanner, humanely euthanized and eliminated from the study.

The animals (n = 6 per dose of LPS; n = 6 controls) were injected with [^{18}F]FEPPA (11.1 MBq; 0.3 mCi) via the tail vein. Dynamic PET images were obtained using a small animal SuperArgus 2r PET (SEDECAL, Madrid, Spain) or 7T PETMR Inline (Bruker, Rheinstetten, Germany) for 30 min with the energy window set to 350-650 keV. Images were acquired every 1 s for 10 images, 10 s for five images, 60 s for nine images, 300 s for two images, and 600 s for 1 image; a total of 27 frames were collected. T1 and T2 MRI were performed to determine the anatomical structure of the brain. The MRI sequences included 0.5-mm thickness coronal T2 Turbo RARE high-resolution

images (TR = 3455 ms, TE = 36 ms, matrix = 256 × 256, average = 8, slice number = 30).

The PET images were reconstructed through three-dimensional ordered-subset expectation maximization. The regional radioactivity concentration (KBq/cc) of [^{18}F]FEPPA was estimated based on the mean pixel values within the volumes of interest (VOI) corresponding to MR images of various regions of the brain. Image data were decay-corrected to the injection time. The radioactivity concentration (KBq/cc) of the VOI was converted to the standard uptake value (SUV) and the mean and standard error of the mean (SEM) radiotracer accumulation values were calculated for various tissues. PET/MR data were analyzed using PMOD 3.7 software (PMOD Technologies Ltd., Zurich, Switzerland).

Quantification of Dynamic PET Imaging Using Logan Graphical Analyses

The Logan graphical method for reversible uptake (40) was used to assess whether [^{18}F]FEPPA PET/CT (30) or PET/MRI could be used to detect differences in the expression of TSPO. Cardiac blood was used as the reference tissue. The slope of the linear portion of the Logan plot represents the total distribution (VT). If metabolite-corrected plasma TACs are not available, a reference region TAC, $C_p(t)$, can be used

instead of the plasma TAC. Then, the slope of the linear portion of the plot can be calculated using (**Eq. 1**)

$$\frac{\int_0^t C_{Tissue}(\tau)d\tau}{C_{Tissue}(t)} = K\frac{\int_0^t C_P(\tau)d\tau}{C_{Tissue}(t)} + V$$

Logan graphical analyses were performed using PMOD 3.7 software.

Real-time reverse transcription-polymerase chain reaction

To assess the transcript levels of the genes encoding the cytokines TNF-α, Il-1β, and Il-6 in the brain following LPS-induced systemic inflammation, total RNA was isolated from the brains of the mice after imaging at the indicated time points after LPS injection. RNA was isolated using the RNeasy Micro Kit (Qiagen, Valencia, CA, USA) and cDNA was prepared using the Super Script III First-Strand Synthesis System Kit (Invitrogen, Carlsbad, CA, USA). RT-qPCR was performed for a total of 40 cycles using a Rotor-Gene Q cycler (Qiagen, Hilden, Germany), according to the manufacturer's protocol using TaqMan gene expression master mix, primers and MGB probe sets (Applied Biosystems, Foster City, CA, USA). The assay IDs for the PCR primer pairs and TaqMan MGB probes were Mm00443260_gl (*Tnf-α*), Mm00434228_ml (*Il-1β*), Mm00446190_ml (*Il-6*) and Mm00607939Msl (*β-actin*). Relative expression levels

were calculated using the comparative threshold cycle (Ct value) method and normalized to the ΔCt of *β-actin*. All analyses were conducted in triplicate.

Western blotting

After imaging, brain tissues were lysed in ice-cold radioimmunoprecipitation assay buffer and total protein lysates were fractionated by sodium dodecyl sulfate-polyacrylamide gel electrophoresis and transferred to polyvinylidene difluoride membranes. The membranes were probed with antibodies against Iba-1, PBR (Cell Signaling Technology, Danvers, MA, USA) and β-actin (Novus Biologicals, Centennial, CO, USA). After washing three times for 10 min in Tris-buffered saline supplemented with 0.1% Tween 20 (TBST), the membranes were incubated with horseradish peroxidase-conjugated secondary antibodies for 1 h, washed with TBST and the signals were visualized and quantified using the GeneGnome Chemiluminescence Imaging System (Syngene, Frederick, MD, USA).

Immunohistochemistry and immunofluorescence

After imaging, the mice were terminally anesthetized, perfused with 4% paraformaldehyde, the brains were dissected, post-fixed overnight in 4% paraformaldehyde at 4 °C, embedded in optimal cutting temperature compound, and

frozen coronal sections (30-μm thick) were prepared. The sections were permeabilized with 1% Triton X-100 in phosphate-buffered saline (PBS) for 10 min, blocked with 1% bovine serum albumin in PBS-T for 1 h, incubated with antibodies against Iba-1 (GeneTex; to detect microglia) and PBR (GeneTex). The sections were incubated with 3'-diaminobenzidine for 20 sec or fluorescein isothiocyanate-conjugated donkey anti-rabbit antibody (1:200) at room temperature for 1 h, and counterstained with 4',6-diamidino-2-phenylindole for 5 min at room temperature.

Paraffin-embedded sections were cut at 5-μm thickness, deparaffinized and rehydrated. Antigen retrieval was carried out by microwaving in 10 mM citrate buffer (pH 6.0) at 100 ºC for 10 min. Sections were washed, incubated in 3% hydrogen peroxide for 15 min at room temperature, incubated in blocking solution for 60 min at room temperature, and incubated overnight with PBR primary antibody (1:50; St John's Laboratory Ltd., London, UK) at 4 ºC. Biotinylated secondary antibodies and 3,3-diaminobenzidine from the Vectastain Elite Kit (Vector Laboratories, Burlingame, CA, USA) were applied according to the manufacturer's protocol.

Immunostained sections were assessed using an AxioScope A1 microscope (Zeiss, Oberkochen, Germany) equipped with a Zeiss Axiocam 512 color digital camera. The IHC images were converted into 8-bit grayscale images in the range [0-255]. The regions of interest (ROI) were manually selected and the intensity of immunostaining

was measured using the software. The median (25%, 75% interquartile range) percentage score for each group was calculated as the average of all mice in each group.

Statistical analysis

Data are expressed as mean ± SEM. One-way ANOVA with the post-hoc Bonferroni or unpaired Student's *t*-test were used for statistical evaluation. $P < 0.05$ was considered statistically significant. Statistical analyses were performed using GraphPad Prism 8 (GraphPad Software, La Jolla, CA, USA).

Results

Automated radiosynthesis of [^{18}F]FEPPA

Fully automated radiosynthesis of [^{18}F]FEPPA was achieved within 80 min. The overall production of [^{18}F]FEPPA was 30 ± 2% (decay-uncorrected, $n = 8$). Specific activity at the end of synthesis ranged from 148.9 to 216.8 GBq/μmol ($n = 8$).

Quality control and stability tests of [^{18}F]FEPPA

The retention time (Rt) of [^{18}F]FEPPA in semi-preparative HPLC was 13.07 min (**Fig. 2A, radio-peak**). The radioactive product was also co-injected with an authentic

FEPPA standard. The retention time (Rt) of [^{18}F]FEPPA (**Fig. 2B, radio-peak**) in HPLC analysis was 6.8 min, which was consistent with that of authentic FEPPA (**Fig. 2C**, **UV peak**).

One typical production batch of [^{18}F]FEPPA was assessed using all of the quality control tests required for human use. In this production, the levels of residual solvents and K2.2.2 were below the levels set by the Taiwan FDA and the values for all other tests all met the specifications for human use.

Quantitative whole-body biodistribution in mice

In vivo dynamic PET/MR imaging was performed in six mice injected with 5 mg/kg LPS and six control mice after administration of [^{18}F]FEPPA. Generally, PET/MR imaging revealed rapid accumulation of [^{18}F]FEPPA in LPS-injected mice, and—to a lesser degree—in the control group (**Fig. 3A**). [^{18}F]FEPPA exhibited biexponential blood clearance kinetics after *i.v.* injection (**Fig. 3B**). The concentration of radioactivity remaining in the blood pool was 1.29 ± 0.03 SUV at 30 min post-injection. Rapid excretion of [^{18}F]FEPPA by the liver was observed. A high concentration of radioactivity was also detected in the kidneys. The pattern of renal clearance was characterized by a rapid increase in radioactivity in the blood and liver, and subsequent clearance by the kidneys. Rapid accumulation of [^{18}F]FEPPA in the lungs, peaking at

1-2 min post-injection, was also observed. The concentration of radioactivity in heart muscle peaked in the first 3 min after injection, and then gradually decreased over time (**Fig. 3B**). Detailed results of the biodistribution of [^{18}F]FEPPA *in vivo* are listed in **Table 1**.

***In vivo* brain region-specific uptake of [^{18}F]FEPPA**

The 3D PET/MRI brain images shown in **Figure 4** illustrate the [^{18}F]FEPPA signals in the control group and LPS groups at 24 h. As shown in **Figure 5**, significantly higher [^{18}F]FEPPA uptake was observed in all brain regions of the LPS group at 24 h compared to the control group. The highest uptake was detected in the hypothalamus, followed by the midbrain, hippocampus, thalamus, brain stem, whole brain, cortex, striatum, cerebellum and amygdala. In control animals, the regional [^{18}F]FEPPA time-activity curves indicated radioactivity peaked during the first 3 min, followed by rapid washout. In contrast, [^{18}F]FEPPA accumulated more rapidly in the brain regions of the LPS group in the first 2-3 min, and then continued to progressively increase to reach a steady state.

Pharmacokinetic characterization of [^{18}F]FEPPA in the brains of LPS-induced mice

The brain regions of the LPS group exhibited significantly higher SUV, VT and AUC values compared to the control mice. Generally, the [^{18}F]FEPPA SUV were significantly different between control and LPS animals from the first 5 min onwards, and the average SUV ratio for all brain regions between the two groups was 1.61 ± 0.1 (**Fig. 6A**).

PET images were quantified using Logan graphical analysis. The VT values for [^{18}F]FEPPA PET in the majority of brain regions were significantly higher in the LPS group than the controls, except for the hypothalamus, brain stem and cerebellum. On average, the [^{18}F]FEPPA VT values were 1.25 ± 0.12-fold higher in the LPS group than the control group (**Fig. 6B**).

Integrated activity (AUC; SUV·min, 0-30 min) revealed rapid cerebral distribution and higher retention of [^{18}F]FEPPA in the LPS group (**Fig. 6C**). The AUC ratio between the LPS and control group was 1.58 ± 0.09. Significantly higher [^{18}F]FEPPA AUCs are consistent with overexpression of the target in the brain of mice injected with LPS, reflecting the well-characterized ability of LPS to induce inflammation and upregulate TSPO.

Quantitative analysis of LPS dose response and brain distribution

To assess whether the [^{18}F]FEPPA uptake dose-response correlates with LPS exposure, we quantified [^{18}F]FEPPA uptake in various brain regions after administration of different doses of LPS. The time-activity curves for various brain regions after injection of LPS are presented in **Figure 7**. There was no significant correlation between [^{18}F]FEPPA uptake and the dose of LPS at concentrations up to 2.5 mg/kg; though the SUV values significantly increased at 5 mg/kg LPS (**Fig. 8**).

LPS stimulates proinflammatory cytokine secretion

To investigate the proinflammatory reaction induced by LPS, we measured the mRNA expression levels of the proinflammatory cytokines TNF-α, IL-1β and IL-6 in brain homogenates at 24 h after injection of LPS. As shown in **Figure 9A**, the mRNAs encoding TNF-α and IL-1β were expressed at higher levels in the brain homogenates of the LPS-group than the control group (LPS 2.5 mg/kg *vs.* control, $P < 0.01$; LPS 5 mg/kg *vs.* control, $P < 0.001$), demonstrating that injection of LPS induced inflammation and the release of proinflammatory cytokines. Thus, we next examined the dose-dependence of cytokine expression and release.

Upregulation of TSPO expression after LPS induction in mice

The TSPO band was detected at 18 kDa in Western blotting (**Fig. 9B**). A marked increase in TSPO expression was observed in the brain 24 h after administration of LPS ($P < 0.05$); Iba-1 expression also increased in the LPS group at this time point ($P < 0.01$; **Fig. 9C**). Western blotting revealed time-dependent induction of TSPO expression, in confirmation of the PET/MR imaging studies.

Quantitative immunostaining confirms the results of *in vivo* PET/CT imaging with [^{18}F]FEPPA

TSPO activity was also analyzed in the brain cortex, hippocampus and cerebellum at 24 h after LPS injection (**Fig. 10A**). TSPO immunoreactivity was significantly higher in the CA1, CA3 and cerebellum at 24 h after administration of LPS, whereas TSPO expression was similar in the CA2 and dentate gyrus between the control and LPS groups. A tendency towards higher expression of TSPO was observed in the cortex of LPS mice; however, this trend was not significant **(Fig. 10B)**.

Cerebral expression of TSPO colocalized with the microglial marker Iba-1 in mice injected with LPS (**Fig. 10C**). Both TSPO and Iba-1 expression were upregulated at 24 h after LPS injection.

Discussion

The aim of this study was to optimize automated radiosynthesis of the TSPO ligand [^{18}F]FEPPA and evaluate the use of [^{18}F]FEPPA to detect neuroinflammation *in vivo*. This work provides the first report of regional-specific distribution of TSPO *in vivo* in the mouse model of systemic LPS challenge. Our results demonstrate [^{18}F]FEPPA rapidly distributed throughout various brain regions and reached a steady-state, which enabled detection of higher regional-specific TSPO expression in the brains of mice injected with LPS. These [^{18}F]FEPPA PET/MRI imaging findings were confirmed by western blotting and immunostaining, which demonstrated increased expression of TSPO in the brain was accompanied by microglial activation. Furthermore, real-time RT-PCR revealed an altered immune balance in the brains of LPS-injected mice, including increased levels of both pro-inflammatory and anti-inflammatory cytokines.

We adapted the manual synthesis reported by Wilson et al. (27) into a reliable, optimized automated [^{18}F]FEPPA radiosynthesis process using the Eckert & Ziegler Modular system. The non-corrected radiochemical yield for the optimized method was 30 ± 2% within 80 min, which is comparable to 39 ± 3% within 34 min (30) and 30 ± 6% within 36 min (41). Quality control confirmed that the [^{18}F]FEPPA product met all current requirements of a radiotracer for human use. The optimized process produces [^{18}F]FEPPA with a consistently high radiochemical purity and specific activity. The

final products of both manual and automated synthesis were stable, maintaining a radiochemical purity of more than 99% at 6 h after the end of synthesis. The process is also economical, as no disposable components are required. Quality control analysis confirmed the identity, strength, quality and purity of the radiocompound, and the stability of the product is sufficient for both animal and clinical studies.

Mice were systemically injected with LPS (5 mg/kg, *i.p.*) to evaluate the optimized [^{18}F]FEPPA for *in vivo* PET/MR imaging. After administration of LPS, visualization of [^{18}F]FEPPA revealed the distribution and expression of TSPO globally increased in the whole body and brain of the mice, in agreement with previous mouse and rat studies (27) (30, 41). Our results also demonstrated that [^{18}F]FEPPA is rapidly and extensively metabolized in the heart, lung and spleen tissues of C57BL6 mice and excreted by the kidneys. PET/MR imaging of [^{18}F]FEPPA in LPS-injected mice indicated high specific binding of the radiolabel to TSPO. Higher radioactive signals were observed in the lung, heart and kidney, which express high levels of TSPO under normal conditions. Furthermore, significant upregulation of TSPO was observed in response to induction of inflammation in the peripheral and central organs in the murine LPS model.

LPS-induced animal models have been widely used to research peripheral inflammation or neuroinflammation in order to identify early diagnosis or treatment/prevention approaches (42) (43). LPS-induced heart injury (10 mg/kg, single

i.p. injection) leads to morphological changes in the myocardium and increases the levels of creatine kinase and lactate dehydrogenase (44). Injection of CD14-deficient (CD14-D) mice (25 mg/kg, single injection, *i.p.*) demonstrated that CD14 mediates the LPS-induced proinflammatory responses in the heart and is required for the development of left ventricular dysfunction during LPS-induced shock (45).

However, only limited preclinical data have been reported on *in vivo* imaging of TSPO in the peripheral tissues. The biodistribution of [^{11}C]PK-11195 PET was first reported in canine and human hearts (46) and [^{123}I]-Iodo-PK11195 SPECT was evaluated in rat hearts (47). [^{18}F]FEDAC PET was used to assess the expression of TSPO (B_{max}) *in vivo* and determine the KD of [^{18}F]FEDAC in peripheral tissues; however, [^{18}F]FEDAC exhibited relatively low signal-to-noise ratio in peripheral tissues such as the heart and lung (48). [^{18}F]FPBMP was subsequently reported, but leads to weak specific signals for TSPO (49). Thus, a quantitative, non-invasive and reliable imaging biomarker for TSPO could enable larger, more reliable preclinical and clinical studies.

Cardiovascular or lung imaging in preclinical studies can be complicated by low scanning efficiency, motion correction for the heart or lungs, and partial volume corrections of radioactivity. The resolution of the PET scanner is also a key limitation. However, PET imaging enables assessment of biological disease processes in the heart

or lungs, whereas magnetic resonance (MR) scanning provides detailed anatomic imaging and tissue characterization. In this study, advanced 7T PET/MR imaging was used to identify the heart muscle and detect significant [^{18}F]FEPPA uptake in the heart muscle 24 h after LPS challenge compared to controls (**Table 1**, $p = 0.05$).

In vivo imaging of TSPO in the peripheral tissues can also help to detect inflammation, such as pneumonia (50) (51). We demonstrated significant [^{18}F]FEPPA uptake in the lungs of LPS-injected mice (**Table 1**, $p = 0.01$). Much lower [^{18}F]FEPPA uptake was observed in the liver and blood, which provided a suitable signal-to-noise ratio for peripheral organs such as the heart muscle and lungs. Hatori et al. evaluated the TSPO radioligand N-benzyl-N-methyl-2-[7,8-dihydro-7-(2-[^{18}F]fluoroethyl)-8-oxo-2-phenyl-9H-purin-9yl]acetamide ([^{18}F]FEDAC) in an acute model of lung injury induced by LPS. In agreement with this study, a similar TAC pattern and clear background were observed in the lungs at 24 h after LPS treatment (52).

Compared to existing non-specific clinical methods such as chest radiography and computed tomography, PET imaging using a TSPO-specific radioligand could potentially provide quantitative information on macrophage trafficking and kinetics in lung diseases, and thus help to evaluate treatment responses and improve our understanding of the pathophysiology of non-infectious inflammatory processes in the lung (53). Non-invasive PET imaging also enables longitudinal assessments (54),

whereas repeat measurements using other invasive methods (e.g., lung biopsy and bronchoalveolar lavage) are unacceptable. The *in vivo* profiles for [^{18}F]FEPPA reached a steady state in the heart muscle and lungs 10 min after injection of [^{18}F]FEPPA, and then gradually decreased (**Fig. 3**). On the one hand, this results demonstrated that [^{18}F]FEPPA significantly increased in peripheral organs or tissues (~3 folds in heart and lung) in the LPS-inducted group as compared to control mice; but on other hand, the fast metabolic rate in plasma (60% metabolite in 30 min imaging time-window) (30) could increase the difficulty of the quantification accuracy of PET imaging and limit its application for the peripheral inflammation.

The brain exhibited relatively lower [^{18}F]FEPPA uptake compared to peripheral organs such as the heart, lung or kidney. Western blotting, real-time PCR and IHC analyses of brain tissue sections for TSPO confirmed the PET/MR imaging detection of significantly higher accumulation of [^{18}F]FEPPA in the brains of mice injected with LPS. To investigate whether the specific binding of [^{18}F]FEPPA in the brain was due to LPS-induced microglial activation, we used western blotting to detect increased co-expression of TSPO and Iba-1 at 24 h after injection of LPS (**Fig. 9**, $p = 0.01$ and $p = 0.05$, respectively).

Regional-specific accumulation of [^{18}F]FEPPA in the brain reflected the changes in TSPO expression. TSPO ligands have been reported to exert beneficial effects as anti-

inflammatory drugs in experimental models of various neurodegenerative diseases and anxiety disorders (55). More than a dozen anti-inflammatory drugs have been developed (55), (56). However, the *in vivo* pharmacokinetic and pharmacodynamics of those anti-inflammatory drugs in specific regions of the brain remain unclear, due to the lack of quantitative or repeatable imaging agents, as described above. In the current study, we used PET/MR-based image segmentation to calculate regional-specific [^{18}F]FEPPA accumulation. At 24 h after injection of LPS, the PET SUV images revealed significant increases in [^{18}F]FEPPA uptake in the majority of brain regions assessed (**Fig. 6A**). A pharmacokinetic parameter, total distribution volume VT, revealed a significant increase in [^{18}F]FEPPA distribution in the various brain regions of LPS-injected mice compared to control mice (**Fig. 6B**). Moreover, the $AUC_{0–30}$ min value for [^{18}F]FEPPA increased by an average of 1.3-fold compared to the controls (**Fig. 6C**). These results are in good agreement with previous publications (30).

LPS in the systemic circulation could induce effects in the CNS by crossing the blood-brain barrier (BBB) and directly activating cells within the CNS. The critical issue of whether LPS actually disrupts the BBB and results in over-estimation of [^{18}F]FEPPA accumulation in the brain was addressed by Vignal et al. (30). Our finding also was in a good agreement that VT represents the most robust parameter for quantifying [^{18}F]FEPPA uptake and is not affected by changes in cerebral blood flow (28).

The poor correlation between the PET signal intensity and the LPS does with TSPO imaging agents in rodent models is also important to consider. Therefore, we performed a LPS dose-response study investigate the effectiveness of [^{18}F]FEPPA. There was no significant difference in brain [^{18}F]FEPPA uptake when the dose of LPS was ≦ 2.5 mg/kg, but significantly higher uptake was observed at 5 mg/kg LPS (**Fig. 9**). Although the levels of cytokines such as tTNF-α, IL-1β andIL-6 in the brain were significantly increased by LPS in a dose-dependent manner (**Fig. 9**, $p < 0.005$~0.001 at 2.5 mg/kg LPS, $p < 0.001$ at 5 mg/kg LPS), these changes could be explained by two factors. A low dose of LPS may cause a certain degree of BBB disruption (57) or systematic daily administration of LPS (0.5 mg/kg consecutively for 6 days) increased expression of TSPO (58) but this may not significantly affect [^{18}F]FEPPA uptake in the brain. Alternatively, this result may indicate the inability of [^{18}F]FEPPA to effectively detect the inflammatory responses induced by low doses of LPS. However, several study conditions should be considered, including the strain of LPS, the mouse strain, the dose, site of injection and time course of LPS administration (acute/single or chronic/multiple injections and duration of treatment), the imaging time-points, sensitivity of the PET detector and the specific activity of the PET agents. PET radioligands that target the TSPO have showed promise in the detection of neuroinflammation, however, their preclinical/clinical utility has been hampered by the

presence of sensitivity of increased TSPO level. Further studies such as coupling imaging of PET [^{18}F]FEPPA and DCE-MRI to assess dose-dependence of LPS on BBB permeability/disruption in rodent model.

Accumulation of radioactivity in the brain or peripheral tissues can be due to the radioligand and its radiometabolite(s). However, the stability or metabolism of the radioligand was not tested using blood or tissue samples in this study. In the metabolite assay reported by Vignal et al., approximately 95% of the parent fraction of unmetabolized [^{18}F]FEPPA in the brain was identified as the intact form at 30 min after injection (30). Therefore, at the imaging time-points 0-30 min after injection, the majority of [^{18}F]FEPPA bound to TSPO in the brain, heart, lung and kidney is likely to be due to [^{18}F] FEPPA.

The presence of TSPO in the brain was confirmed by Western blotting. In comparison to controls, TSPO and the microglial marker Iba-1 were expressed at significantly higher levels in the brain at 24 h after LPS injection (**Fig. 10C**, $P < 0.05$). Based on IHC, cerebral TSPO expression colocalized with Iba-1 (a microglial marker) in LPS-injected mice, consistent with previous findings (59) (60). Thus, TSPO represents a suitable molecular target to modulate microglia/macrophage function during neuroinflammation. Moreover, TSPO expression was assessed in various brain

tissues. Quantitative analysis of immunohistological staining demonstrated that TSPO was significantly upregulated in the CA1, CA3 and cerebellum by LPS (**Fig. 10**).

Conclusions

The second-generation TSPO radioligand [^{18}F]FEPPA has been extensively used in clinical or preclinical development to study neuroinflammation and peripheral-type inflammation. We optimized an automated radiosynthesis method on the Eckert & Ziegler Modular system that meets cGMP requirements and produces [^{18}F]FEPPA at high purity and high yield. The experimental evidence in this study indicates [^{18}F]FEPPA can be employed to monitor neuroinflammatory processes *in vivo* using PET. [^{18}F]FEPPA uptake/binding were quantified in various anatomical brain regions, and ligand detected significant increased TSPO levels in the brain of systemic LPS-induced neuroinflammation (5 mg/kg). Therefore, these developments may enable promising animal or human studies on TSPO-related neuroinflammation.

List of abbreviations

7T PET/MR: 7-Tesla Positron emission tomography/ Magnetic resonance imaging

[^{18}F]FEPPA: [18F]-N-(2-(2-Fluoroethoxy)benzyl)-N-(4-phenoxypyridin-3-yl)

AUC: Area under curve

CK: creatine kinase

CNS: central nervous system

Il-1β: Interleukin 1 beta

Il-6: interleukin-6

LDH: lactate dehydrogenase

LPS: Lipopolysaccharides

PBR: peripheral-type benzodiazepine receptor

RT-PCT: Real-time reverse transcription-polymerase chain reaction

SEM: standard error of the mean

SPECT: Single-photon emission computed tomography

SUV: Standard uptake value

TAC: time-activity curve

TNF-α: tumor necrosis factor Alpha

TSPO: translocator protein 18ka

VT: total volume of distribution

Declarations

Ethics approval and consent to participate

Not applicable

Consent for publication

Not applicable

Availability of data and material

The datasets used and/or analyzed during the current study are available from the corresponding author on reasonable request.

Competing interests

The authors declare that they have no competing interests.

Funding

Funding for this study was provided by Ministry of Science and Technology R.O.C. (MOST 106-2314-B-010 -012 -MY3, MOST 106-2314-B-075 -014 -MY3, MOST 107-2314-B-532 -003 -MY3), Medical Affairs Bureau of the Ministry of National Defense, Taiwan (MAB-108-053) and The Featured Areas Research Center Program within the framework of the Higher Education Sprout Project by the Ministry of Education (MOE) in Taiwan.

Authors' contributions

Study design: Skye Hsin-Hsien Yeh, Wen-Sheng Huang.

Synthesis Precursor for Radiolabeling and Radiolabeling: Chi-Wei Chang, Ya-Yao Huang, Chyng-Yann Shiue.

In vivo PET/CT or PET/MRI imaging: Chuang-Hsin Chiu, Tsung-Hsun Yu, Yu-Yeh Kuo.

In vitro study: Hung-Ming Wu

Histology: Pao-Yeh Wang, Ming Hsien Lin.

Manuscript writing: Skye Hsin-Hsien Yeh, Chi-Wei Chang.

Acknowledgements

We thank the Molecular Imaging Facility Small Animal 7T PET/MR and Brain Research Center at National Yang-Ming University for the technical support.

References

1. Liu GJ, Middleton RJ, Hatty CR, Kam WW, Chan R, Pham T, et al. The 18 kDa translocator protein, microglia and neuroinflammation. Brain Pathol. 2014;24(6):631-53.
2. Denora N, Natile G. An Updated View of Translocator Protein (TSPO). Int J Mol Sci. 2017;18(12).
3. Banati RB. Visualising microglial activation in vivo. Glia. 2002;40(2):206-17.
4. Beinlich A, Strohmeier R, Kaufmann M, Kuhl H. Relation of cell proliferation to expression of peripheral benzodiazepine receptors in human breast cancer cell lines. Biochem Pharmacol. 2000;60(3):397-402.
5. Anholt RR, Pedersen PL, De Souza EB, Snyder SH. The peripheral-type benzodiazepine receptor. Localization to the mitochondrial outer membrane. J Biol Chem. 1986;261(2):576-83.
6. Antkiewicz-Michaluk L, Guidotti A, Krueger KE. Molecular characterization and mitochondrial density of a recognition site for peripheral-type benzodiazepine ligands. Mol Pharmacol. 1988;34(3):272-8.
7. Chen MK, Guilarte TR. Translocator protein 18 kDa (TSPO): molecular sensor of brain injury and repair. Pharmacol Ther. 2008;118(1):1-17.
8. Cagnin A, Brooks DJ, Kennedy AM, Gunn RN, Myers R, Turkheimer FE, et al. In-vivo measurement of activated microglia in dementia. Lancet. 2001;358(9280):461-7.
9. Pavese N, Gerhard A, Tai YF, Ho AK, Turkheimer F, Barker RA, et al. Microglial activation correlates with severity in Huntington disease: a clinical and PET study. Neurology. 2006;66(11):1638-43.
10. Gerhard A, Neumaier B, Elitok E, Glatting G, Ries V, Tomczak R, et al. In vivo imaging of activated microglia using [11C]PK11195 and positron emission tomography in patients after ischemic stroke. Neuroreport. 2000;11(13):2957-60.
11. Versijpt J, Debruyne JC, Van Laere KJ, De Vos F, Keppens J, Strijckmans K, et al. Microglial imaging with positron emission tomography and atrophy measurements with magnetic resonance imaging in multiple sclerosis: a correlative study. Mult Scler. 2005;11(2):127-34.
12. Gershen LD, Zanotti-Fregonara P, Dustin IH, Liow JS, Hirvonen J, Kreisl WC, et al. Neuroinflammation in Temporal Lobe Epilepsy Measured Using Positron Emission Tomographic Imaging of Translocator Protein. JAMA Neurol. 2015;72(8):882-8.

13. Banati RB, Goerres GW, Myers R, Gunn RN, Turkheimer FE, Kreutzberg GW, et al. [11C](R)-PK11195 positron emission tomography imaging of activated microglia in vivo in Rasmussen's encephalitis. Neurology. 1999;53(9):2199-203.
14. Boutin H, Chauveau F, Thominiaux C, Kuhnast B, Gregoire MC, Jan S, et al. In vivo imaging of brain lesions with [(11)C]CLINME, a new PET radioligand of peripheral benzodiazepine receptors. Glia. 2007;55(14):1459-68.
15. Venneti S, Lopresti BJ, Wang G, Slagel SL, Mason NS, Mathis CA, et al. A comparison of the high-affinity peripheral benzodiazepine receptor ligands DAA1106 and (R)-PK11195 in rat models of neuroinflammation: implications for PET imaging of microglial activation. J Neurochem. 2007;102(6):2118-31.
16. Chauveau F, Boutin H, Van Camp N, Thominiaux C, Hantraye P, Rivron L, et al. In vivo imaging of neuroinflammation in the rodent brain with [11C]SSR180575, a novel indoleacetamide radioligand of the translocator protein (18 kDa). Eur J Nucl Med Mol Imaging. 2011;38(3):509-14.
17. Lavisse S, Guillermier M, Herard AS, Petit F, Delahaye M, Van Camp N, et al. Reactive astrocytes overexpress TSPO and are detected by TSPO positron emission tomography imaging. J Neurosci. 2012;32(32):10809-18.
18. Zhang MR, Maeda J, Ogawa M, Noguchi J, Ito T, Yoshida Y, et al. Development of a new radioligand, N-(5-fluoro-2-phenoxyphenyl)-N-(2-[18F]fluoroethyl-5-methoxybenzyl)acetamide, for pet imaging of peripheral benzodiazepine receptor in primate brain. J Med Chem. 2004;47(9):2228-35.
19. Takano A, Piehl F, Hillert J, Varrone A, Nag S, Gulyas B, et al. In vivo TSPO imaging in patients with multiple sclerosis: a brain PET study with [18F]FEDAA1106. EJNMMI Res. 2013;3(1):30.
20. Imaizumi M, Briard E, Zoghbi SS, Gourley JP, Hong J, Musachio JL, et al. Kinetic evaluation in nonhuman primates of two new PET ligands for peripheral benzodiazepine receptors in brain. Synapse. 2007;61(8):595-605.
21. Dickstein LP, Zoghbi SS, Fujimura Y, Imaizumi M, Zhang Y, Pike VW, et al. Comparison of 18F- and 11C-labeled aryloxyanilide analogs to measure translocator protein in human brain using positron emission tomography. Eur J Nucl Med Mol Imaging. 2011;38(2):352-7.
22. Guo Q, Colasanti A, Owen DR, Onega M, Kamalakaran A, Bennacef I, et al. Quantification of the specific translocator protein signal of 18F-PBR111 in healthy humans: a genetic polymorphism effect on in vivo binding. J Nucl Med. 2013;54(11):1915-23.
23. Imaizumi M, Briard E, Zoghbi SS, Gourley JP, Hong J, Fujimura Y, et al. Brain and whole-body imaging in nonhuman primates of [11C]PBR28, a promising PET

radioligand for peripheral benzodiazepine receptors. Neuroimage. 2008;39(3):1289-98.
24. Chauveau F, Van Camp N, Dolle F, Kuhnast B, Hinnen F, Damont A, et al. Comparative evaluation of the translocator protein radioligands 11C-DPA-713, 18F-DPA-714, and 11C-PK11195 in a rat model of acute neuroinflammation. J Nucl Med. 2009;50(3):468-76.
25. Peyronneau MA, Saba W, Goutal S, Damont A, Dolle F, Kassiou M, et al. Metabolism and quantification of [(18)F]DPA-714, a new TSPO positron emission tomography radioligand. Drug Metab Dispos. 2013;41(1):122-31.
26. Yui J, Maeda J, Kumata K, Kawamura K, Yanamoto K, Hatori A, et al. 18F-FEAC and 18F-FEDAC: PET of the monkey brain and imaging of translocator protein (18 kDa) in the infarcted rat brain. J Nucl Med. 2010;51(8):1301-9.
27. Wilson AA, Garcia A, Parkes J, McCormick P, Stephenson KA, Houle S, et al. Radiosynthesis and initial evaluation of [18F]-FEPPA for PET imaging of peripheral benzodiazepine receptors. Nucl Med Biol. 2008;35(3):305-14.
28. Rusjan PM, Wilson AA, Bloomfield PM, Vitcu I, Meyer JH, Houle S, et al. Quantitation of translocator protein binding in human brain with the novel radioligand [18F]-FEPPA and positron emission tomography. J Cereb Blood Flow Metab. 2011;31(8):1807-16.
29. Mizrahi R, Rusjan PM, Vitcu I, Ng A, Wilson AA, Houle S, et al. Whole body biodistribution and radiation dosimetry in humans of a new PET ligand, [(18)F]-FEPPA, to image translocator protein (18 kDa). Mol Imaging Biol. 2013;15(3):353-9.
30. Vignal N, Cisternino S, Rizzo-Padoin N, San C, Hontonnou F, Gele T, et al. [(18)F]FEPPA a TSPO Radioligand: Optimized Radiosynthesis and Evaluation as a PET Radiotracer for Brain Inflammation in a Peripheral LPS-Injected Mouse Model. Molecules. 2018;23(6).
31. Zanotti-Fregonara P, Veronese M, Pascual B, Rostomily RC, Turkheimer F, Masdeu JC. The validity of (18)F-GE180 as a TSPO imaging agent. Eur J Nucl Med Mol Imaging. 2019;46(6):1205-7.
32. Turner MR, Cagnin A, Turkheimer FE, Miller CC, Shaw CE, Brooks DJ, et al. Evidence of widespread cerebral microglial activation in amyotrophic lateral sclerosis: an [11C](R)-PK11195 positron emission tomography study. Neurobiol Dis. 2004;15(3):601-9.
33. Politis M, Lahiri N, Niccolini F, Su P, Wu K, Giannetti P, et al. Increased central microglial activation associated with peripheral cytokine levels in premanifest Huntington's disease gene carriers. Neurobiol Dis. 2015;83:115-21.

34. Golla SS, Boellaard R, Oikonen V, Hoffmann A, van Berckel BN, Windhorst AD, et al. Quantification of [18F]DPA-714 binding in the human brain: initial studies in healthy controls and Alzheimer's disease patients. J Cereb Blood Flow Metab. 2015;35(5):766-72.
35. Varrone A, Mattsson P, Forsberg A, Takano A, Nag S, Gulyas B, et al. In vivo imaging of the 18-kDa translocator protein (TSPO) with [18F]FEDAA1106 and PET does not show increased binding in Alzheimer's disease patients. Eur J Nucl Med Mol Imaging. 2013;40(6):921-31.
36. Ory D, Celen S, Verbruggen A, Bormans G. PET radioligands for in vivo visualization of neuroinflammation. Curr Pharm Des. 2014;20(37):5897-913.
37. Ory D, Planas A, Dresselaers T, Gsell W, Postnov A, Celen S, et al. PET imaging of TSPO in a rat model of local neuroinflammation induced by intracerebral injection of lipopolysaccharide. Nucl Med Biol. 2015;42(10):753-61.
38. Dickens AM, Vainio S, Marjamaki P, Johansson J, Lehtiniemi P, Rokka J, et al. Detection of microglial activation in an acute model of neuroinflammation using PET and radiotracers 11C-(R)-PK11195 and 18F-GE-180. J Nucl Med. 2014;55(3):466-72.
39. Sridharan S, Lepelletier FX, Trigg W, Banister S, Reekie T, Kassiou M, et al. Comparative Evaluation of Three TSPO PET Radiotracers in a LPS-Induced Model of Mild Neuroinflammation in Rats. Mol Imaging Biol. 2017;19(1):77-89.
40. Logan J. Graphical analysis of PET data applied to reversible and irreversible tracers. Nucl Med Biol. 2000;27(7):661-70.
41. Vasdev N, Green DE, Vines DC, McLarty K, McCormick PN, Moran MD, et al. Positron-emission tomography imaging of the TSPO with [(18)F]FEPPA in a preclinical breast cancer model. Cancer Biother Radiopharm. 2013;28(3):254-9.
42. Catorce MN, Gevorkian G. LPS-induced Murine Neuroinflammation Model: Main Features and Suitability for Pre-clinical Assessment of Nutraceuticals. Curr Neuropharmacol. 2016;14(2):155-64.
43. Largeau B, Dupont AC, Guilloteau D, Santiago-Ribeiro MJ, Arlicot N. TSPO PET Imaging: From Microglial Activation to Peripheral Sterile Inflammatory Diseases? Contrast Media Mol Imaging. 2017;2017:6592139.
44. Xianchu L, Lan Z, Ming L, Yanzhi M. Protective effects of rutin on lipopolysaccharide-induced heart injury in mice. J Toxicol Sci. 2018;43(5):329-37.
45. Knuefermann P, Nemoto S, Misra A, Nozaki N, Defreitas G, Goyert SM, et al. CD14-deficient mice are protected against lipopolysaccharide-induced cardiac inflammation and left ventricular dysfunction. Circulation. 2002;106(20):2608-15.

46. Charbonneau P, Syrota A, Crouzel C, Valois JM, Prenant C, Crouzel M. Peripheral-type benzodiazepine receptors in the living heart characterized by positron emission tomography. Circulation. 1986;73(3):476-83.
47. Gildersleeve DL, Van Dort ME, Johnson JW, Sherman PS, Wieland DM. Synthesis and evaluation of [123I]-iodo-PK11195 for mapping peripheral-type benzodiazepine receptors (omega 3) in heart. Nucl Med Biol. 1996;23(1):23-8.
48. Yanamoto K, Kumata K, Fujinaga M, Nengaki N, Takei M, Wakizaka H, et al. In vivo imaging and quantitative analysis of TSPO in rat peripheral tissues using small-animal PET with [18F]FEDAC. Nucl Med Biol. 2010;37(7):853-60.
49. Anjani K. Tiwari JY, Yiding Zhang, Masayuki Fujinaga,Tomoteru Yamasaki, Lin Xie,NYoko Shimoda, Katsushi Kumata, Akiko Hatoria and Ming-Rong Zhang. . [18F]FPBMP: – a potential new positron emission tomography radioligand for imaging of translocator protein (18 kDa) in peripheral organs of rats. RSC Advances. 2015;5(123).
50. Hardwick MJ, Chen MK, Baidoo K, Pomper MG, Guilarte TR. In vivo imaging of peripheral benzodiazepine receptors in mouse lungs: a biomarker of inflammation. Mol Imaging. 2005;4(4):432-8.
51. Wang H, Pullambhatla M, Guilarte TR, Mease RC, Pomper MG. Synthesis of [(125)I]iodoDPA-713: a new probe for imaging inflammation. Biochem Biophys Res Commun. 2009;389(1):80-3.
52. Hatori A, Yui J, Yamasaki T, Xie L, Kumata K, Fujinaga M, et al. PET imaging of lung inflammation with [18F]FEDAC, a radioligand for translocator protein (18 kDa). PLoS One. 2012;7(9):e45065.
53. Capitanio S, Nordin AJ, Noraini AR, Rossetti C. PET/CT in nononcological lung diseases: current applications and future perspectives. Eur Respir Rev. 2016;25(141):247-58.
54. Branley HM, du Bois RM, Wells AU, Jones HA. PET scanning of macrophages in patients with scleroderma fibrosing alveolitis. Nucl Med Biol. 2008;35(8):901-9.
55. Lee Y, Park Y, Nam H, Lee JW, Yu SW. Translocator protein (TSPO): the new story of the old protein in neuroinflammation. BMB Rep. 2020;53(1):20-7.
56. Monga S, Nagler R, Amara R, Weizman A, Gavish M. Inhibitory Effects of the Two Novel TSPO Ligands 2-Cl-MGV-1 and MGV-1 on LPS-induced Microglial Activation. Cells. 2019;8(5).
57. Banks WA, Gray AM, Erickson MA, Salameh TS, Damodarasamy M, Sheibani N, et al. Lipopolysaccharide-induced blood-brain barrier disruption: roles of cyclooxygenase, oxidative stress, neuroinflammation, and elements of the neurovascular unit. J Neuroinflammation. 2015;12:223.

58. Wang W, Zhang L, Zhang X, Xue R, Li L, Zhao W, et al. Lentiviral-Mediated Overexpression of the 18 kDa Translocator Protein (TSPO) in the Hippocampal Dentate Gyrus Ameliorates LPS-Induced Cognitive Impairment in Mice. Front Pharmacol. 2016;7:384.
59. Bonsack Ft, Alleyne CH, Jr., Sukumari-Ramesh S. Augmented expression of TSPO after intracerebral hemorrhage: a role in inflammation? J Neuroinflammation. 2016;13(1):151.
60. Pannell M, Economopoulos V, Wilson TC, Kersemans V, Isenegger PG, Larkin JR, et al. Imaging of translocator protein upregulation is selective for pro-inflammatory polarized astrocytes and microglia. Glia. 2020;68(2):280-97.

Tables

Table 1: Biodistribution of accumulated radioactivity (SUV) in various tissues at the designed time points after administration of [^{18}F]FEPPA. Data are mean ± SEM; *p < 0.05, **p < 0.01, One-way ANOVA with Bonferroni *post hoc* test.

Tissues	Control	LPS
Blood	1.29 ± 0.03	1.29 ± 0.128
Heart muscle	1.24 ± 0.06	3.60 ± 0.722*
Liver	1.48 ± 0.36	1.60 ± 0.097
Lung	1.38 ± 0.08	3.60 ± 0.722**
Spleen	1.16 ± 0.32	0.96 ± 0.443
Kidney	4.80 ± 0.57	5.86 ± 0.504
Whole brain	0.48 ± 0.05	0.76 ± 0.014

Figure Legends

Figure 1: [^{18}F]FEPPA radiosynthesis on the Eckert & Ziegler modular system. [^{18}F]FEPPA was synthesized using an in-house reaction sequence; the reagents used in the automated procedure are listed in **Suppl.Table 1**.

Figure 2: (A) The retention time (Rt) of [^{18}F]FEPPA in semi-preparative HPLC analysis was 13.07 min. **(B)** The retention time (Rt) of [^{18}F]FEPPA in HPLC analysis was 6.8 min. **(C)** The retention time (Rt) of authentic FEPPA in HPLC analysis was 6.6 min.

Figure 3: (A) Representative whole-body coronal PET/MR images of [^{18}F]FEPPA in control and LPS-injected animals. PET images were generated by summation of the whole scan (0–30 min) and color-coded to the range of SUV values. **(B)**Time activity curves for [^{18}F]FEPPA radioactivity (SUV) in blood, heart muscle, liver, lung, spleen and kidney. Data are mean ± SEM.

Figure 4: 3D PET/MRI images of the brain obtained 30 min after *i.v.* administration of [^{18}F]FEPPA in control and LPS-injected animals. Significantly higher [^{18}F]FEPPA

uptake was observed in all brain regions of the LPS group at 24 h compared to the control group. Images are color-coded to the range of SUV values.

Figure 5: Time-activity curves for animal PET/MR studies of [^{18}F]FEPPA for the control group and 24 h after LPS injection. Data are mean ± SEM.

Figure 6: Pharmacokinetics of [^{18}F]FEPPA after *i.v.* administration. Quantitative analysis of radioactivity in control mice and LPS-injected mice. (A) SUV, (B) VT, and (C) AUC. Data are mean ± SEM; *$p < 0.05$, **$p < 0.01$.

Figure. 7: Time-activity curves for [^{18}F]FEPPA in different regions of the brain based on PET/MRI imaging 24 h after injection of various does of LPS. Data are mean ± SEM.

Figure 8: [^{18}F]FEPPA SUV for various brain regions in control mice and mice injected with different of doses LPS. Data are mean ± SEM; *$p < 0.05$, **$p < 0.01$, **$p < 0.001$, One-way ANOVA with Bonferroni *post hoc* test.

Figure 9: **(A)** Cytokine mRNA expression levels of TNF-α, Il-1β and Il-6 in the the brain tissues 24 h after LPS injection. **(B)** the levels of Iba-1 and TSPO at 3 and 24 h

after injection of 5 mg/kg LPS determined by immunoblots, **(C)** Quantitative analysis of protein levels of immunoblots. Data are mean ± SEM ($n = 3$ mice/group); *$p < 0.05$, **$p < 0.01$, ***$p < 0.005$.

Figure 10: **(A)** Immunostaining of the cortex, CA1, CA2, CA3, DG and cerebellum for TSPO. Scale bar: 100 µm. **(B)** Intensity of TSPO immunostaining in six selected brain regions of control and LPS-injected mice: CTX-Cortex, CA1, CA2, CA3, DG—hippocampus, CRE-cerebellum. (C) Expression of TSPO (green) colocalized with the microglia marker Iba-1 (red). Scale bar: 20 µm. * $p < 0.05$, ** $p < 0.01$.

Supplementary Table

Suppl.Table 1: List of reagents used in the automated procedure.

Vial number	Reagents	Volumes
vial A	Recovered $H_2{}^{18}O$	
vial B	Eluent QMA (K_2CO_3/K222 in CH_3CN/H_2O, 44/11, v/v)	1 mL
vial C	CH_3CN anhydrous	0.8 mL
vial D	CH_3CN anhydrous	0.8 mL
vial E	Mobile phase (1/1 CH_3CN /H_2O + 0.5% phosphoric acid)	2 mL
vial F	Precursor	5 mg
vial G	Collect reaction mixture	
vial H	H_2O (to mix with the collected LC fraction)	40 mL
vial I	H_2O (to remove CH3CN)	15 mL
vial J	Ethanol	0.9 mL
vial K	Normal saline	5 mL
vial L	sterile vial containing 5 ml saline (for collecting product)	
vial M	Mobile phase (1/1 CH_3CN /H_2O + 0.5% phosphoric acid)	

Figures

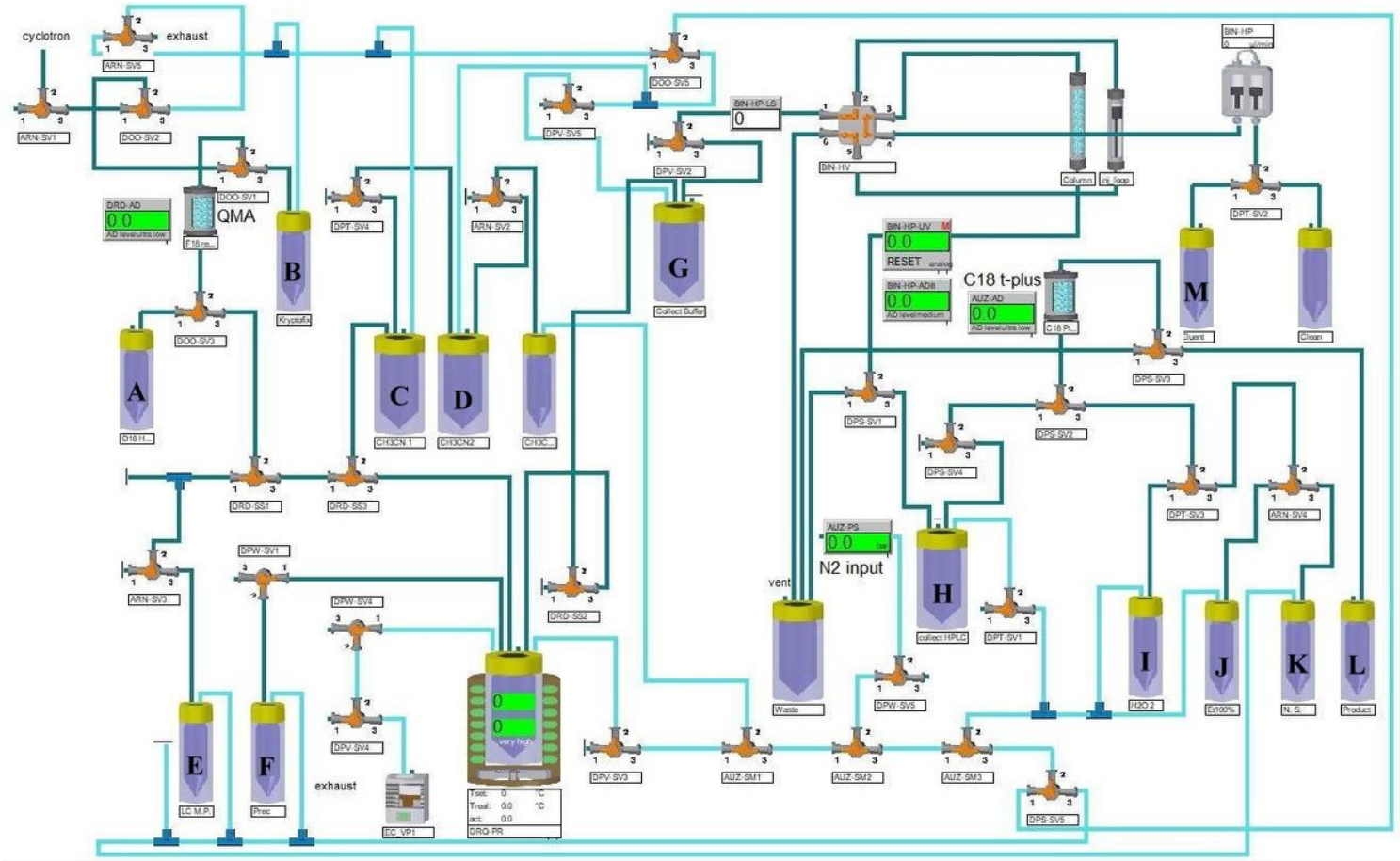

Figure 1

[18F]FEPPA radiosynthesis on the Eckert & Ziegler modular system. [18F]FEPPA was synthesized using an in-house reaction sequence; the reagents used in the automated procedure are listed in Suppl.Table 1.

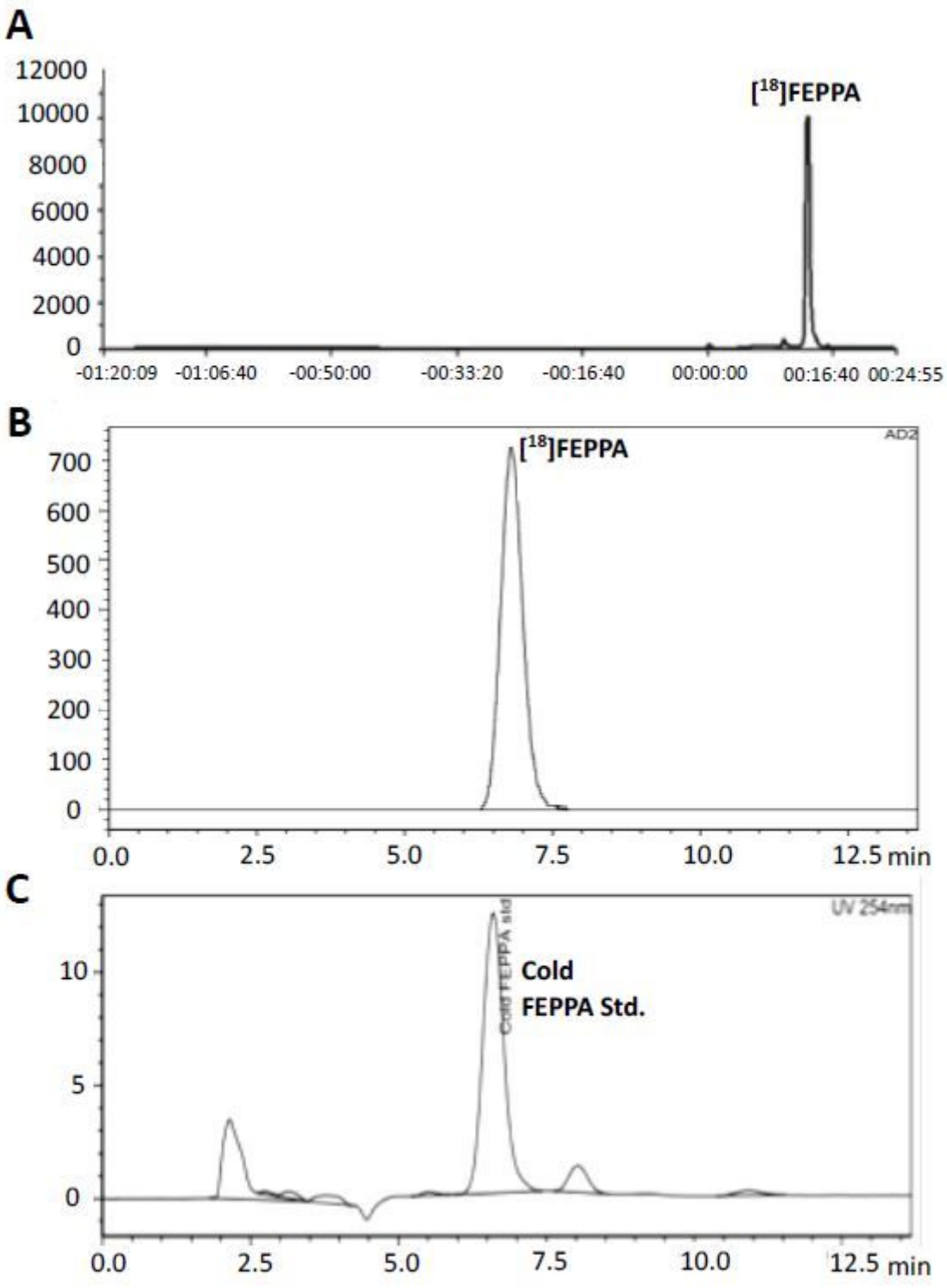

Figure 2

(A) The retention time (Rt) of [18F]FEPPA in semi-preparative HPLC analysis was 13.07 min. (B) The retention time (Rt) of [18F]FEPPA in HPLC analysis was 6.8 min. (C) The retention time (Rt) of authentic FEPPA in HPLC analysis was 6.6 min.

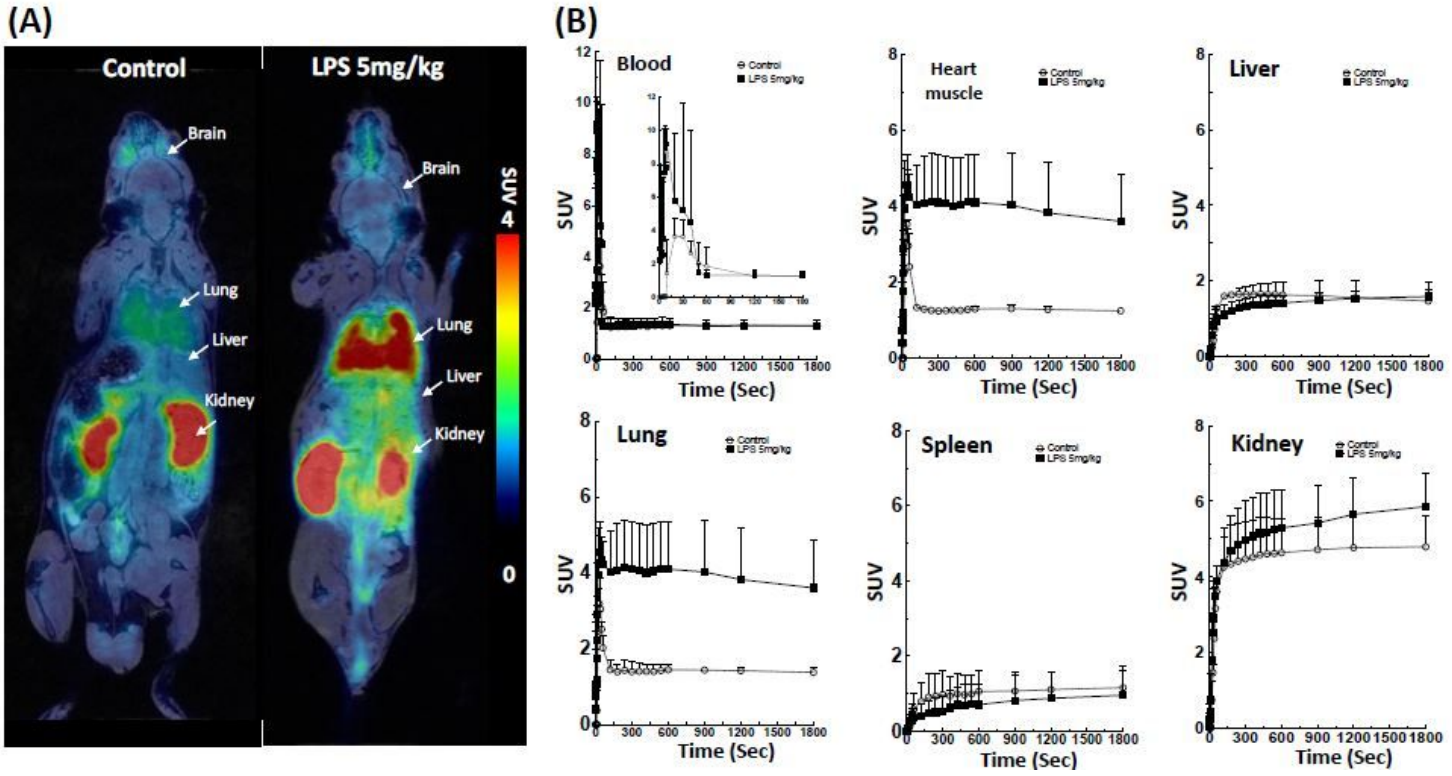

Figure 3

(A)Representative whole-body coronal PET/MR images of [18F]FEPPA in control and LPS-injected animals. PET images were generated by summation of the whole scan (0–30 min) and color-coded to the range of SUV values. (B)Time activity curves for [18F]FEPPA radioactivity (SUV) in blood, heart muscle, liver, lung, spleen and kidney. Data are mean ± SEM.

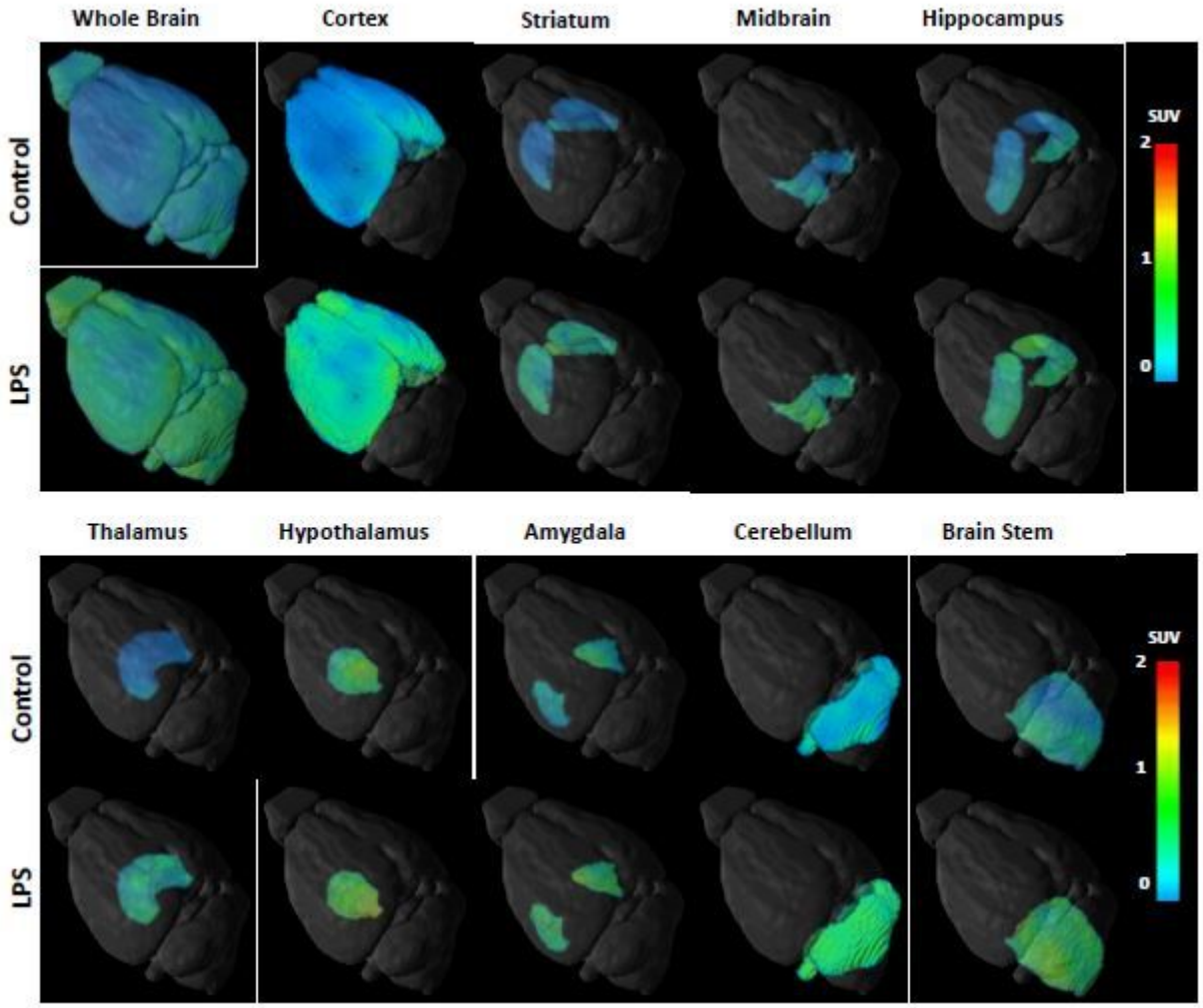

Figure 4

3D PET/MRI images of the brain obtained 30 min after i.v. administration of [18F]FEPPA in control and LPS-injected animals. Significantly higher [18F]FEPPA uptake was observed in all brain regions of the LPS group at 24 h compared to the control group. Images are color-coded to the range of SUV values.

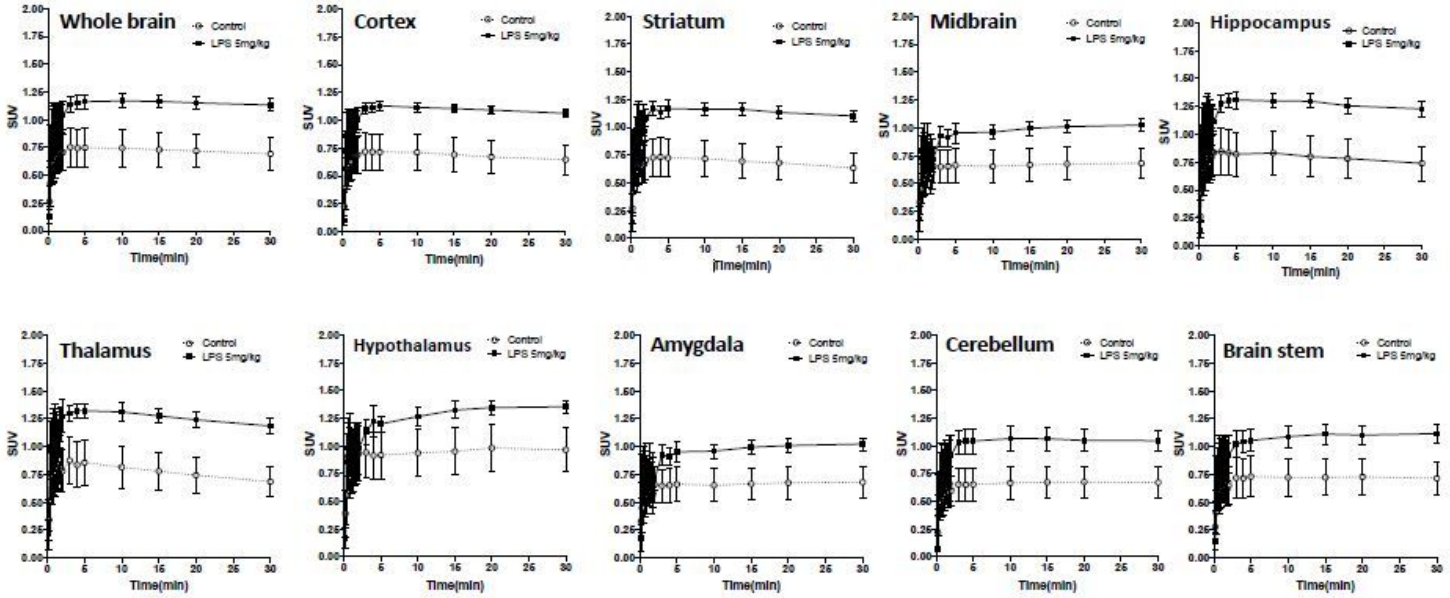

Figure 5

Time-activity curves for animal PET/MR studies of [18F]FEPPA for the control group and 24 h after LPS injection. Data are mean ± SEM.

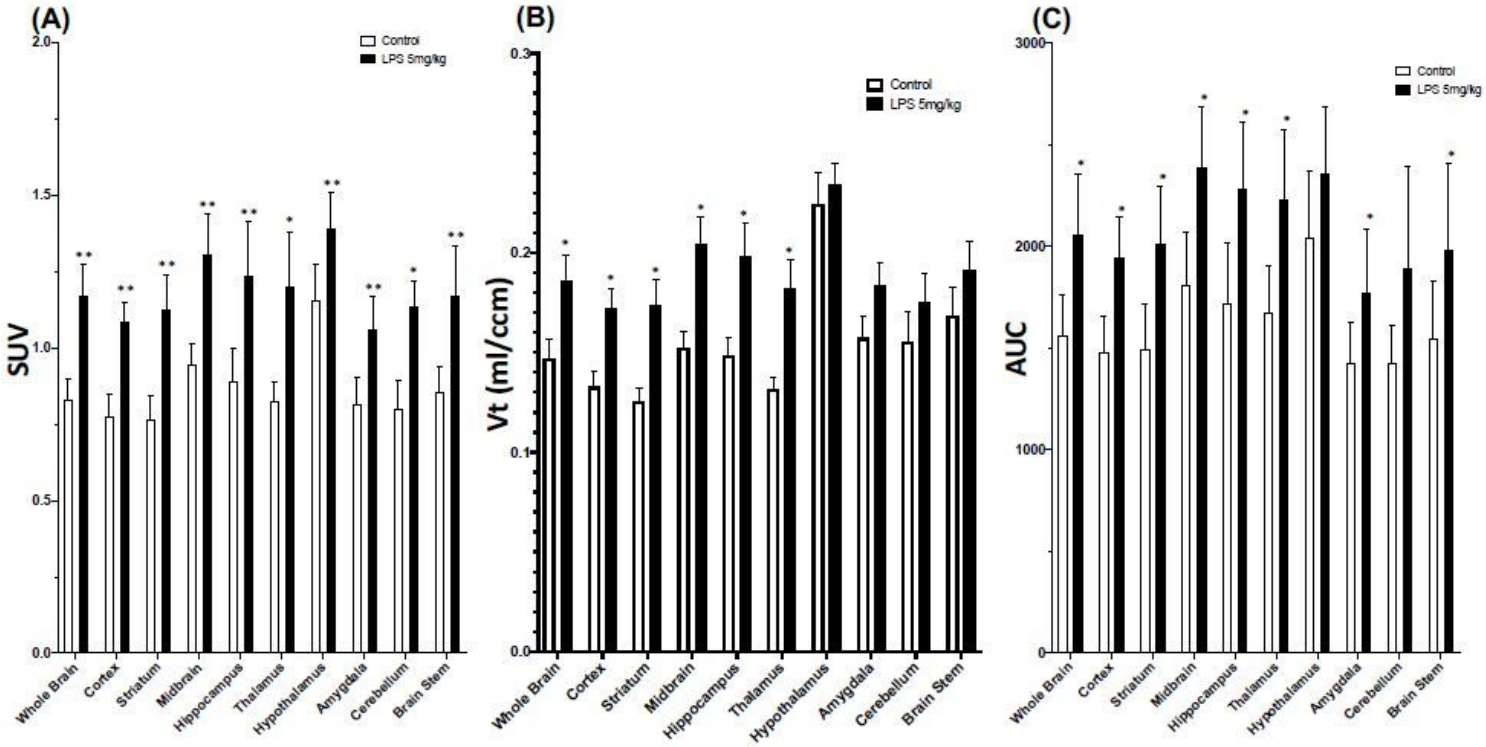

Figure 6

Pharmacokinetics of [18F]FEPPA after i.v. administration. Quantitative analysis of radioactivity in control mice and LPS-injected mice. (A) SUV, (B) VT, and (C) AUC. Data are mean ± SEM; *p < 0.05, **p < 0.01.

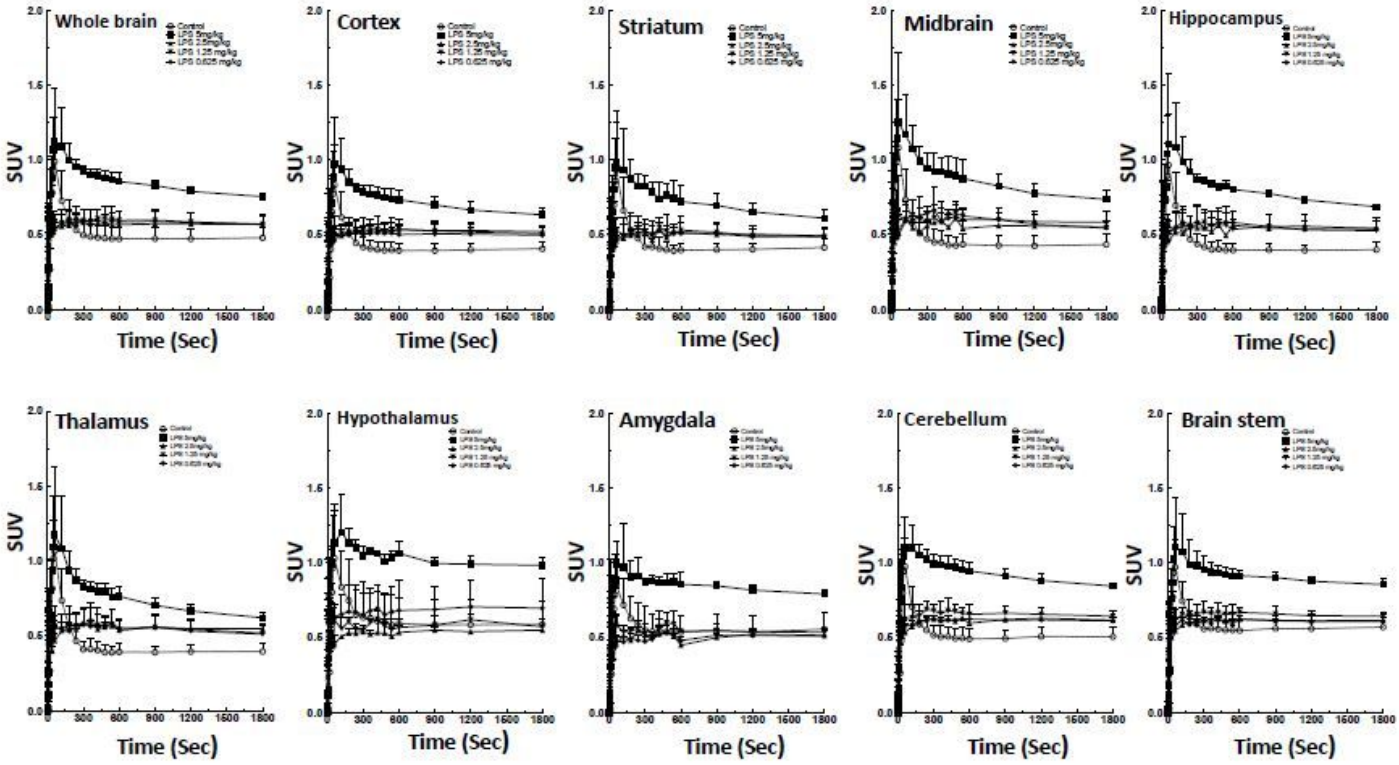

Figure 7

Time-activity curves for [18F]FEPPA in different regions of the brain based on PET/MRI imaging 24 h after injection of various does of LPS. Data are mean ± SEM.

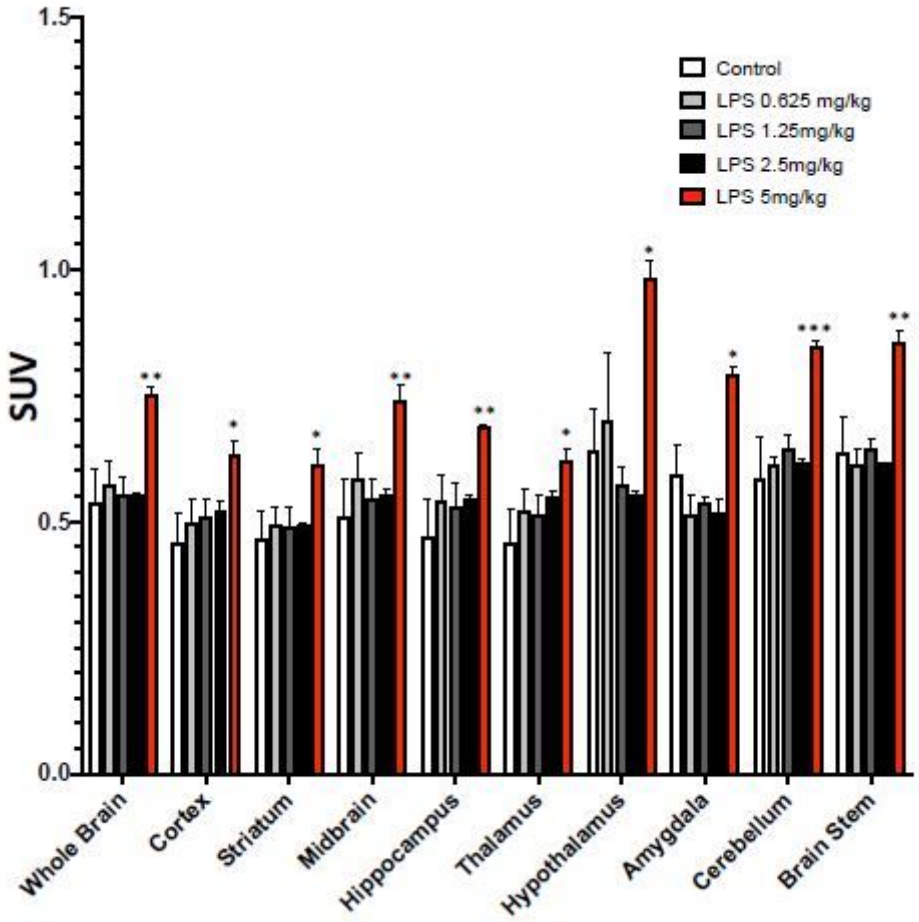

Figure 8

[18F]FEPPA SUV for various brain regions in control mice and mice injected with different of doses LPS. Data are mean ± SEM; *p < 0.05, **p < 0.01, **p < 0.001, One-way ANOVA with Bonferroni post hoc test.

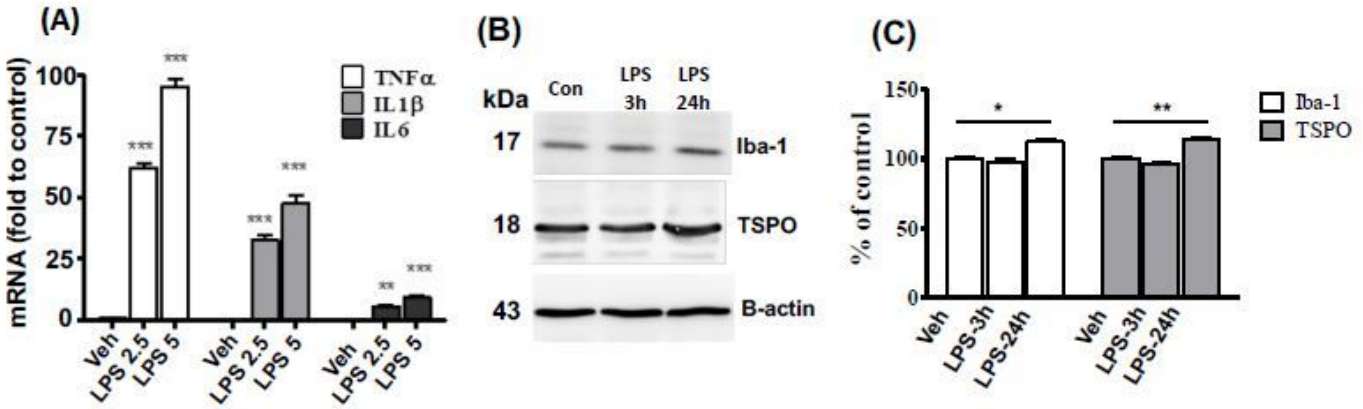

Figure 9

(A) Cytokine mRNA expression levels of TNF-α, Il-1β and Il-6 in the the brain tissues 24 h after LPS injection. (B) the levels of Iba-1 and TSPO at 3 and 24 h after injection of 5 mg/kg LPS determined by immunoblots, (C) Quantitative analysis of protein levels of immunoblots. Data are mean ± SEM (n = 3 mice/group); *p < 0.05, **p < 0.01, ***p < 0.005.

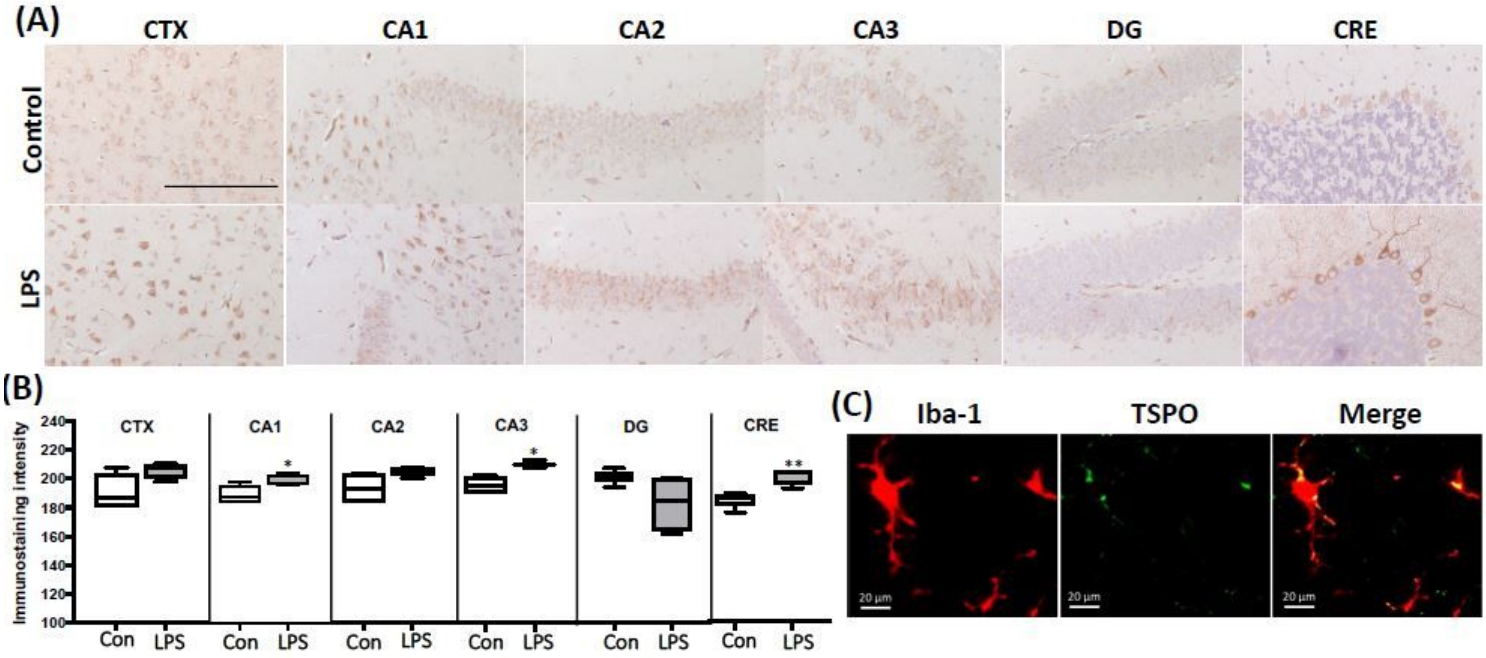

Figure 10

(A) Immunostaining of the cortex, CA1, CA2, CA3, DG and cerebellum for TSPO. Scale bar: 100 µm. (B) Intensity of TSPO immunostaining in six selected brain regions of control and LPS-injected mice: CTX-Cortex, CA1, CA2, CA3, DG—hippocampus, CRE-cerebellum. (C) Expression of TSPO (green) colocalized with the microglia marker Iba-1 (red). Scale bar: 20 µm. * p < 0.05, ** p < 0.01.

Supplementary Files

This is a list of supplementary files associated with this preprint. Click to download.

- SupplementaryTable.docx